



HAL
open science

A dual experimental / numerical approach to understand delamination of oxide scale during indentation test

Victor Claverie–Burgué, Pierre Montmitonnet, Inal Karim, Alain Burr, Michel Picard, Amico Settefrati

► To cite this version:

Victor Claverie–Burgué, Pierre Montmitonnet, Inal Karim, Alain Burr, Michel Picard, et al.. A dual experimental / numerical approach to understand delamination of oxide scale during indentation test. 25e Congrès Français de Mécanique, Aug 2022, Nantes, France. hal-04281711

HAL Id: hal-04281711

<https://hal.science/hal-04281711>

Submitted on 13 Nov 2023

HAL is a multi-disciplinary open access archive for the deposit and dissemination of scientific research documents, whether they are published or not. The documents may come from teaching and research institutions in France or abroad, or from public or private research centers.

L'archive ouverte pluridisciplinaire **HAL**, est destinée au dépôt et à la diffusion de documents scientifiques de niveau recherche, publiés ou non, émanant des établissements d'enseignement et de recherche français ou étrangers, des laboratoires publics ou privés.

A dual experimental / numerical approach to understand delamination of oxide scale during indentation test

V. CLAVERIE—BURGUE^{a, b}, P. MONTMITONNET^a,
K. INAL^a, A. BURR^a,
M. PICARD^b, A. SETTEFRATI^b

a. MINES Paris, PSL Research University, Centre de mise en forme des matériaux (CEMEF), CNRS [UMR 7635], 06904 Sophia Antipolis Cedex, France

Email : victor.claverie-burgue@mines-paristech.fr,

b. ArcelorMittal Maizières Research SA , Voie Romaine, 57280 Maizières-lès-Metz, France

Mots clés: low carbon steel, indentation, Adhesion, CZM, thin film, oxidation

Résumé :

Durant le laminage à chaud, une couche d'oxyde croît à la surface de l'acier. Pour limiter ces défauts de surface, des cages de décalaminage sont introduites dans la chaîne de production pour enlever cette couche. L'idée de cette étude consiste à évaluer les propriétés de l'oxyde et de son interface en utilisant la micro-indentation pour mieux comprendre le décalaminage. Pour cela, des échantillons d'acier bas carbone sont oxydés puis indentés à température ambiante. En fonction de l'aire délaminiée, mesurée sur des coupes FIB (Focused Ion Beam), l'énergie interfaciale d'adhésion de l'oxyde est calculée à l'aide d'un modèle analytique. Des simulations par éléments finis (Abaqus®) du procédé d'indentation sont effectuées pour affiner la compréhension de la fissuration. Dans un premier temps, une analyse des contraintes est réalisée sous l'hypothèse d'un milieu restant continu ; elle permet d'expliquer la présence de tous les types de fissures observées. Dans un second temps, un modèle CZM (Modèle de Zone Cohésive) est utilisé pour simuler la délamination de l'oxyde lors de l'indentation ; il permet de préciser le déroulement de la fissuration, qui est confronté avec ce que l'expérience révèle post-mortem.

Abstract:

During the hot rolling process, an oxide scale grows at the surface of steel. Descaling stands are added in the production line to remove this scale and avoid the defects it may induce. The aim of this project is to evaluate the oxide and its interface properties using micro-indentation to better understand descaling. Oxidized low carbon samples are indented at room temperature. Measuring delamination width using FIB (Focused Ion Beam) cross sections and thanks to an analytical model, interfacial adhesion value is calculated. Finite elements simulations of indentation on ABAQUS® complete the

understanding of interface fracture. First, assuming the steel-oxide continuity is maintained, a stress analysis explains all the types of cracks detected in experiments. Then CZM (Cohesive Zone Modelling) is used to allow delamination of oxide during indentation. The interfacial fracture scheme it discloses is confronted with what experiments reveal post-mortem.

1. Introduction

During the hot rolling process, low carbon steel slabs are heated at high temperature (1200°C) to be made softer (reduction of the roll load) and more deformable. All along this process, an oxide scale is produced on the surface of the slabs (~10-100µm). It consists of three components: Wustite $Fe_{1-x}O$ (~90%) in contact with the steel, an intermediate layer of Magnetite Fe_3O_4 (~8%) and a thin layer at the surface (~2%) of Hematite Fe_2O_3 [1]. This scale has to be removed to avoid surface defects. Therefore, descaling stands are added in the production line and water jets are sent (150 bar) on the scale to produce mechanical and thermal stresses and make the oxide layer crack and spall [2,3]. The work reported here is a part of a study, which consists in designing and carrying out experiments at high temperature to understand the oxide behaviour during descaling. Indeed, oxide scale undergoes a ductile-brittle transition which has an influence on the oxide behaviour at high temperature [4,5,6,7].

In this article, only room temperature experiments and simulations are presented to confirm the capability of the dual approach to respond to the industrial descaling process. Among all characterisation techniques, indentation is chosen to activate delamination mechanism, the one that is essential in descaling [2]. Indeed, this approach allows characterization of both oxide and steel and its interface, which is essential to determine a stress-based fracture criterion relevant for the computation of descaling. Several models have been developed to evaluate adhesion of thin film on a substrate [8,9,10,11,12,13]. In the past years, CZM (cohesive zone models) have been widely used in order to model fracture of thin film and more precisely to describe delamination behaviour [14,15,16,17,18].

First, Room Temperature (RT) indentation of pre-oxidized samples are presented, and FIB cutting on indentation marks are used to measure interfacial toughness. ABAQUS® software indentation model is described, using CZM elements at the interface between steel and oxide. Influence of parameters are finally discussed and comparison with experimental work is done.

2 Experimental

2.1 Indentation tests

Low carbon steel (IF: Interstitial Free and HSLA: High Strength Low Alloy) samples are manually polished with a SiC abrasive paper (granulometry 22 µm) and oxidized in a controlled atmosphere furnace at 650°C or 700°C. After cooling to room temperature, indentation is carried out using a homemade micro-indentation tester (from 0.1N to 30N). In surface, “circular” cracks are observed using a Scanning Electron Microscopy (SEM, MAIA3, Tescan), see Figure 1a. Literature reports strong influence of substrate during indentation tests of thin film. Indeed, for low force indentation (when ratio

between penetration of indenter on thickness of oxide ($p/t < 0.1$), no cracks are present because plastic strain is restrained to the oxide.

To observe degradation at the interface between steel and oxide, cross-sections are prepared using a Xe plasma Focus Ion Beam (FIB) thanks to a FIB column mounted on a SEM (Tescan FERA3 dual beam microscope). Figure 1b shows:

- 1) in reality, circular cracks deviate outwards and do not propagate to the interface with steel.
- 2) delamination is observed below indentation.
- 3) normal cracks starting perpendicular to the interface are also present. This is due to the oxide layer bending following plastic deformation of steel; fracture occurs on the extrados.

All these fracture mechanisms are reproducible and independent on oxide thickness.

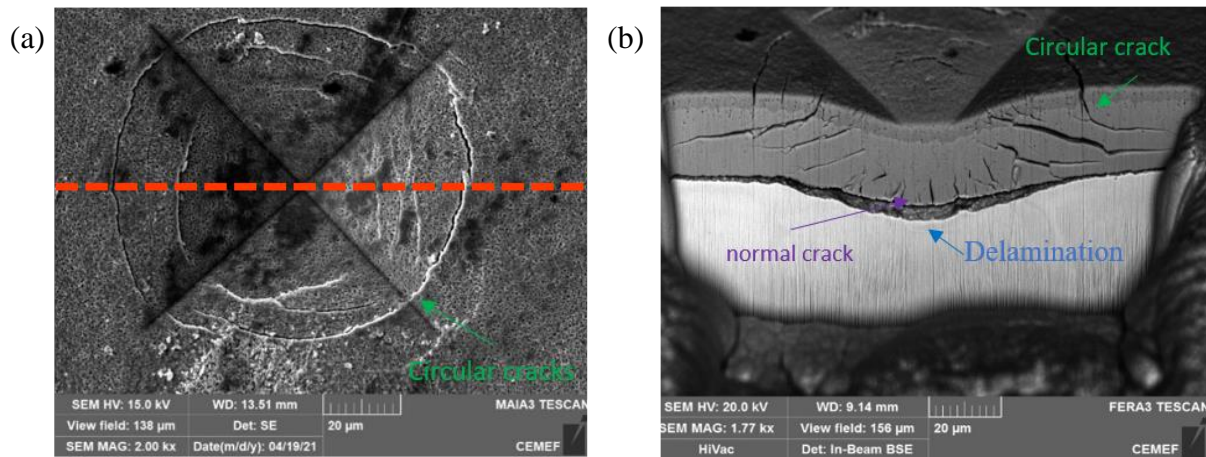


Figure 1 : SEM observation of oxidized IF specimen (thickness 26 μm) indentation with 5N force ($p/t \sim 0.6$). (a) top view showing circular cracks. (b) cross-section of the indentation, prepared by milling the imprint along the red-line, perpendicular to the top surface.

2.2 Adhesion values

Adhesion of a thin film is controlled by interfacial bonding strength. Indentation is used to stress the interface and generate delamination. G , the energy release rate, is the drop of strain energy in the system brought about by a unit increase of crack surface area. It is related to the stress intensity factor K (proportional to the load) by $G = K^2/E$. G provides the energy needed to create new surface (surface energy γ , plus some inelastic strain energy if needed to propagate the crack (plasticity or viscoelasticity at crack tip). In case of non-dissipative, elastic behaviour, equilibrium propagation implies that $G = 2\gamma$. Therefore, following crack propagation provides a quantitative determination of interface energy. Different models of thin film delamination have been reported [8,19]. Rosenfeld et al. [9] determine interfacial fracture energy of epoxy coating on soda-lime glass substrate by considering that debond crack is driven by contact stresses during loading. This model is efficient when the delaminated area is an annulus of inner radius a , the contact radius, and outer radius c (crack extension). The interfacial adhesion energy G is given by:

$$G = \frac{2(1 - \nu_c^2)\sigma_{rb}^2 h_c}{E_c} \left[1 - \nu_c + (1 - \nu_c) \left(\frac{c}{a} \right)^2 \right]^{-2} \quad (1)$$

with E_c and ν_c are the Young's modulus and Poisson's ratio of the thin film, h_c its thickness. σ_{rb} is the radial stress at the outer edge of the contact zone at full load; it is calculated by applying the Tresca yield criterion to the plastically deformed zone contact. The authors assumed that $\sigma_{rb} = \sigma_{yc} - H_c$ where σ_{yc} is the yield stress and H_c is the hardness of the coating and an approximation of the hydrostatic stress. The H_c/σ_{yc} ratio is approximately 3.

The exploitation of this analytical model is based on debond crack size measurements. For each grade at least 5 imprints are considered. Adhesion calculated value are detailed in Table 1. Difference between grades is explained by alloying elements, at the interface, enrichment of some elements (C, Si and Mn) tends to strongly degrade adhesion. Large heterogeneity for adhesion value is found, it is inherent to oxide adhesion measurement. Similar results were found in literature with others mechanical tests for oxide [20,21,22,23,24]. These results are more precisely detailed and discussed in another article [33].

Grade	G_c (J/m ²)	
	Average	Min-Max
IF	336 ± 39	287 – 474
HSLA	45 ± 30	0 – 136

Table 1 : Adhesion value calculated for two grades IF and HSLA.

3 Numerical study

3.1 Simulation parameters

Indentation tests on oxide at room temperature indicate that multiple cracking occurs. To have a better understanding of experimental work, numerical simulations are launched to observe stress field and relate it with delamination of oxide at the interface. This dual approach was widely used on thin film [15,17,18,25,26]. Here, axis-symmetry is assumed to reduce calculation time. Indenter angle is therefore 71.3° (Vickers equivalent). A computation volume of 250 μm (radius) x 100 μm (thickness) was found sufficient to avoid edge effects. To reproduce the experimental tests presented in Figure 1, oxide thickness is set to 26 μm . Reference node is localized at the top of the indenter; a displacement of 15 μm is applied in the negative z direction. The indenter is considered as a rigid body for simplicity due to its high hardness and modulus. Fixed-boundary conditions are applied to the substrate and right side of sample. The same mesh density is used in oxide and steel (0.5 μm), and 4-node bilinear axisymmetric quadrilateral elements with reduced integration are selected. Interaction between indenter and oxide is specified as master-slave surface (indenter is master) with friction $\mu_m = 0.1$ (Coulomb model) imposed by a penalty technique and unilateral contact normal behaviour (hard contact and separation allowed after contact). Both the loading and the unloading are simulated. To simplify, oxide is considered as a single homogeneous phase, whereas in reality, it may consist of 2 or 3 sublayers, moreover sometimes porous and fractured; such complexity is left for future studies. Oxide and steel are considered with an elasto-visco-plastic behaviour. The Young's moduli of the oxide and the steel at room temperature are respectively 240 GPa and 210 GPa [27], both Poisson's coefficients are 0.3. The visco-plastic part follows a Hollomon-type model where K is the consistency, the strain hardening exponent is n and the strain rate sensitivity coefficient is m :

$$\sigma = K \cdot \varepsilon^n \cdot \dot{\varepsilon}^m \quad (2)$$

For steel, K value is directly calculated using Tabor's formula [28], considering that flow stress is equal to Vickers Hardness divided by three for a representative strain of 0.08. As ratio of hardness between oxide and steel at room temperature is equal to 3.4 ($Hv_{\text{steel}} = 1.9 \text{ GPa}$, $Hv_{\text{oxide}} = 6.5 \text{ GPa}$), the assumption is made that $K_{\text{oxide}} = 3 K_{\text{steel}}$. For steel, m is set as 0.01 and $n=0.152$ in agreement with data calculated by Picqué using 4 point bending tests on low carbon steel [7]. For oxide, a strong assumption is made by which the n and m coefficients are chosen identical to those of steel. All parameters used are indicated in Table 2.

Material law Parameter	Steel	Oxide
K (MPa)	1076	3230
n	0.152	0.152
m	0.01	0.01
E (GPa)	210	240
Poisson's coefficient	0.3	0.3

Table 2 : Material parameters used in numerical simulation

3.2 CZM parameters

Experimental results show delamination at the interface. Cohesive elements are added in simulation at the interface between oxide and steel. It allows progressive damage and failure in a cohesive layer whose response is defined in terms of Traction-Separation law (T-S law) (Figure 2)

These models are based on three steps directly observable on T-S law:

- elastic behaviour of cohesive elements
- initiation of crack
- propagation and damage of elements

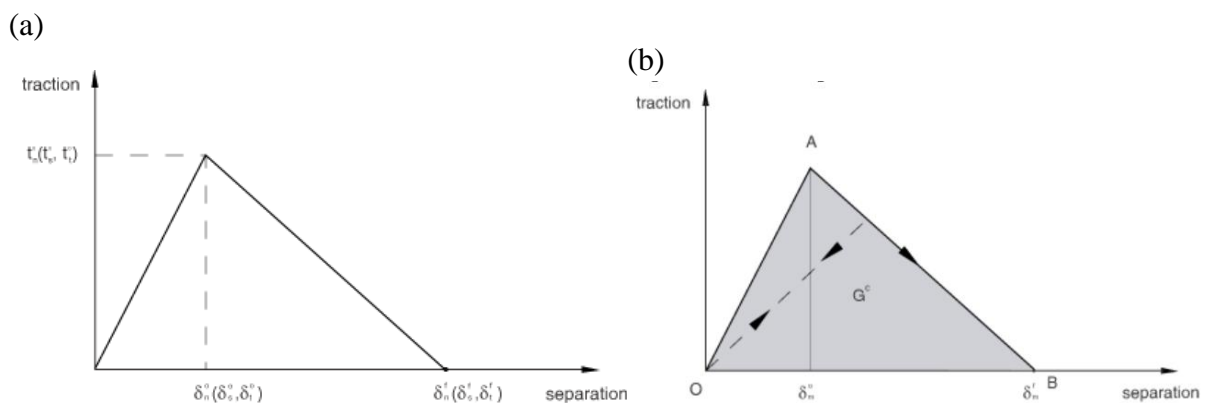


Figure 2: a) Typical traction separation law b) evolution of degradation of CZM elements in case of non-monotonic loading (extracted from Abaqus documentation)

The first slope is defined as the stiffness of CZM elements, the reaction of elements is considered as elastic. For oxide/steel interface, these elastic values are taken equal to the Young's modulus of steel: $E=G_1=G_2=210 \text{ GPa}$. Then, damage initiation refers to the beginning of degradation of interface, at the

top of the T-S law (point A in Figure 2 b). When stress components (t_n (normal) or t_s and t_t (shear)) in cohesive elements reach their critical values t_n^0 , t_s^0 and t_t^0 damage begins. The criterion chosen is that the maximum nominal stress ratio (as defined in the expression below) reaches a value of one:

$$\max\left\{\frac{t_n}{t_n^0}, \frac{t_s}{t_s^0}, \frac{t_t}{t_t^0}\right\} = 1 \quad (3)$$

with t_n , t_s , and t_t stress value in cohesive elements and t_n^0 , t_s^0 and t_t^0 the respective critical stresses. Here, to begin with, $t_n^0 = t_s^0 = t_t^0 = 200$ MPa, according to Noh et al. [29]]. Once criterion is reached, damage evolution law describes the rate at which cohesive elements are degraded. Damage evolution can be defined based on the energy that is dissipated as a result of the damage process, also called the fracture energy. The fracture energy is equal to the area under the traction-separation curve (Figure 2 b)). A scalar damage variable, D , represents the overall damage in the material. It varies from 0 (undamaged) to 1 (cohesive elements are destroyed, and crack is propagated, point B in Figure 2 b). Here, damage evolution is modelled with a linear softening, D is equal to:

$$D = \frac{\delta_m^f (\delta_m^{fmax} - \delta_m^0)}{\delta_m^{max} (\delta_m^f - \delta_m^0)} \quad (4)$$

where $\delta_m^f = 2G_c/T_{eff}^0$ with T_{eff}^0 as the effective traction at damage initiation. δ_m^{max} refers to the maximum value of the effective displacement attained during the loading history. The stress components of the traction-separation model are affected by the damage according to:

$$t_n = (1 - D)\bar{t}_n \quad t_s = (1 - D)\bar{t}_s \quad t_t = (1 - D)\bar{t}_t \quad (5)$$

where \bar{t}_n , \bar{t}_s and \bar{t}_t are the stress components predicted by the elastic traction-separation behaviour for the current strains without damage. The degradation mode is set to a mixed mode, it would suggest a mix of both normal and shear deformation. In our first simulation, G_c is selected in agreement with experimental work (330 J/m^2) for IF grade. In the Figure 3, 4-node axisymmetric cohesive element are used, meshing is adapted to have same number of elements in oxide, steel and interface (Figure 3).

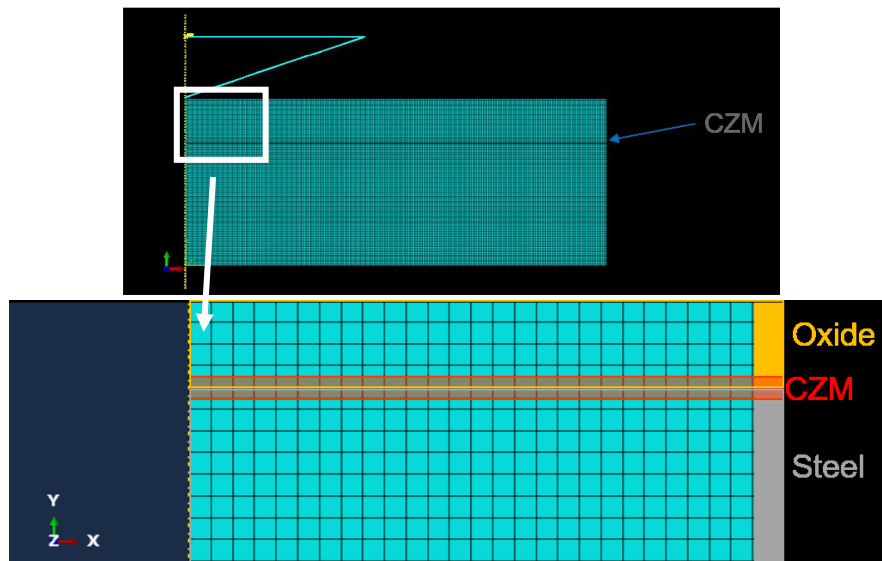


Figure 3: Localisation of CZM at the interface between oxide and steel

4 Results of simulation

4.1 Continuum simulation (without CZM elements)

Before analysing the damaged interface, it is useful to observe stress field to point out zone where failure may happen and compare with experimental fractures. In this case, the area of contact of indenter is $37 \mu\text{m}$ for a penetration of $15 \mu\text{m}$. In surface, both σ_{11} (radial : Figure 4 a) and σ_{33} (circumferential : Figure 4 c) stress component are in tension near the contact edge, and are increasing all along the loading to 1700 MPa. At room temperature, we observed circular cracks in this zone; tensile σ_{11} explains the circular cracks. We have observed experimentally that circular cracks are not propagated until the interface: from a certain stage of oxide bending, a compression area is present at the interface on the σ_{11} map, below the edge of indentation. This bending field (surface in tension and compression at the interface) channels crack outward more and more, quasi-horizontally. At the interface, values of normal stress are largely compressive (Figure 4 b)). The shearing component is larger just below indentation contact edge $r = a$ (at the end of indentation, $a = 37 \mu\text{m}$). It reaches the interface with a high value, the maximum being a few μm closer to the axis $r = 36 \mu\text{m}$ (Figure 4 d)). This point stress moves as the indentation and scans the interface outwards. It is seen that delamination is likely to initiate where this component is maximal ($\sim 500 \text{ MPa}$), and delamination behaviour remains in mode II.

Finally, a zone with weak radial tension is found below the indenter, $r < a/2$. It is probably connected with the cracks normal to the interface found in experiments. Here, the largest tension is just below the upper surface, at indenter tip apex. Experimentally, these cracks start from the interface. At this stage, it is not possible to decide if and how they could be connected with delamination.

During unloading, we have found no stress component evolution suggesting further crack initiation or propagation.

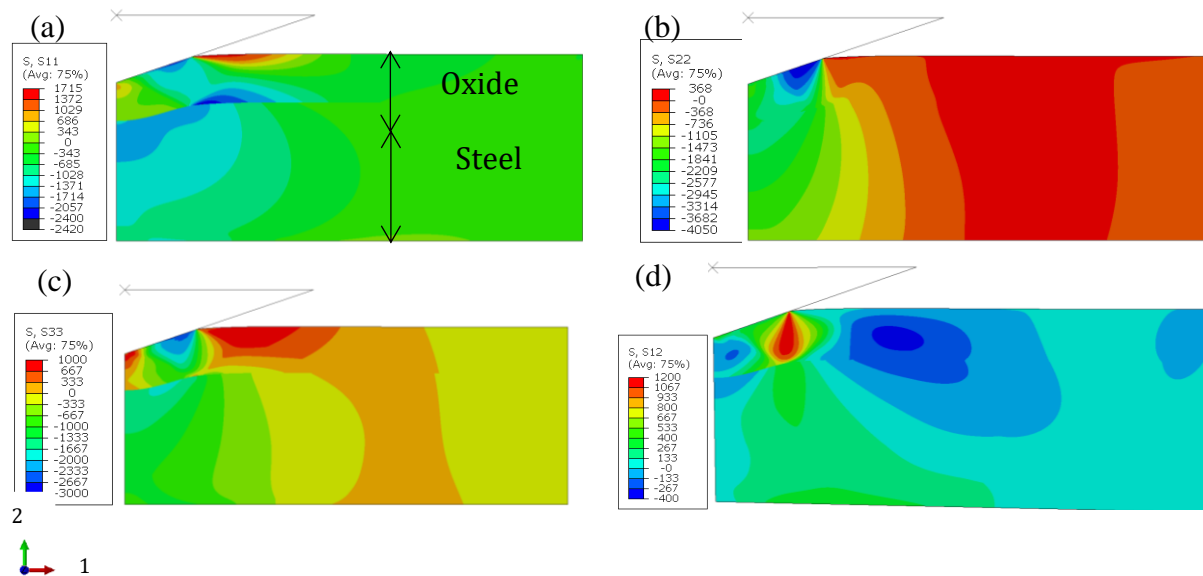


Figure 4: Stress distribution at the end of loading of Vickers indentation (5 N) of an oxidized steel sample (thickness of oxide: $26 \mu\text{m}$). Indentation depth $15 \mu\text{m}$ ($p/t = 0.6$). (a) 11 (radial) component, (b) 22 (normal) component, (c) 33 (circumferential) component (d) 12 shearing component,

Note that initial internal stresses have not been considered. Generally in oxide, compressive residual stresses are present due to both thermal stresses (differential dilatation) during cooling and growth stresses [30]. They may influence results [31]. At room temperature, X-Ray diffraction analysis showed the presence of an in-plane stress $\sim -150 \text{ MPa}$ in the present oxide layer. This is well below the stress

level found in these simulations and probably small enough to avoid major interference, but this should be checked in the future.

4.2 Simulations with CZM elements at the interface

Previous simulations are essential to assume zone where cracks are the most liable to appear. They have shown risks of interfacial as well as normal, circular cracks. Figure 5 shows evolution of shearing component during all along the loading. At the beginning of indentation, for $p/t < 0.1$, the shearing band is strictly confined inside the oxide (Figure 5 a). By increasing penetration to $11\mu\text{m}$, this band and reaches interface (Figure 5 b), delamination of oxide is starting. Thus, the evolution of stresses in CZM elements at the interface confirmed that shearing component is the source of delamination. A detailed comparison between cases with and without CZM shows that shearing stress value at the interface are the same with CZM elements at the end of the loading (Figure 5 c) to compare with Figure 4 d).

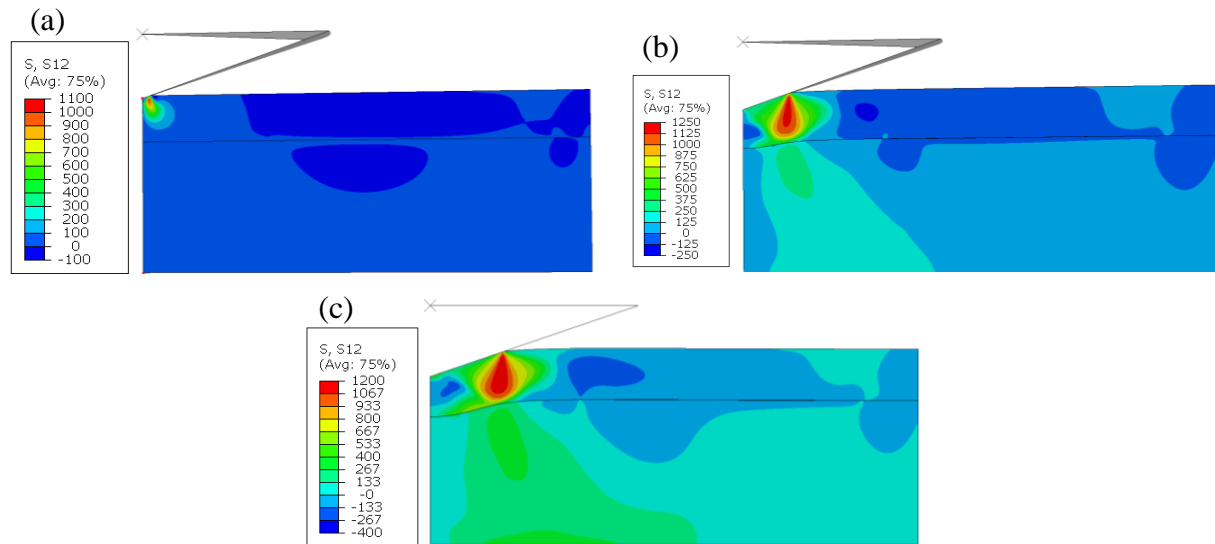


Figure 5: Stress distribution at the interface: σ_{12} shearing component, (a) after a penetration of $2,5\mu\text{m}$ $p/t=0.1$ (b) after a penetration of $11.7\mu\text{m}$ when delamination is starting $p/t=0.42$ (c) at the end of loading of depth $15\mu\text{m}$, $p/t = 0.6$.

In order to identify the delaminated area, the scalar stiffness degradation variable SDEG is observed, when SDEG is equal to 1, interface has cracked (Figure 6). The left part of crack is called c_1 and the right part c_2 . The index i refers to the initiation of cracking and f to the final position of the crack at the end of indentation test.

As expected, in cohesive elements, this value reached 1 after 70% of the total loading, when shearing component is equal to 200 MPa. It is interesting to note that the first cohesive element destroyed is at a distance $r = 18\mu\text{m}$ from the symmetry axis and initially $c_{1i} = 15\mu\text{m}$ and $c_{2i} = 21\mu\text{m}$. All along the present simulations, as soon as initiation criterion is reached, complete degradation occurs, evolution of D from 0 to 1 is very fast, this means that the first part of the T-S law (elastic until the critical stress) controls delamination. The influence of these parameters is discussed later. Interfacial crack extends smoothly during all the loading, up to $c_{1f} = 14\mu\text{m}$ and $c_{2f} = 35\mu\text{m}$. Delaminated area after loading and unloading are the same. This confirms Rosenfeld' assumption that interfacial crack grows only during loading [9].

This means that this kind of crack does not propagate during unloading, contrary to e.g. lateral cracks in bulk brittle material indentation which are known to form at the end of unloading [32].

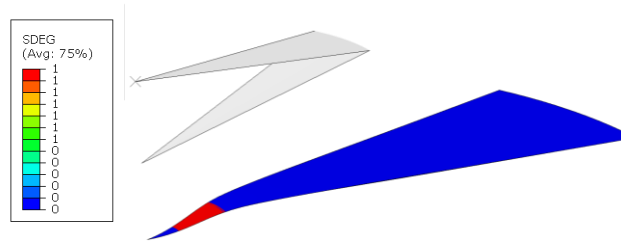


Figure 6: SDEG value of degraded CZM elements ($D = 1$, red) at the interface after loading (indentation radius $a = 37 \mu\text{m}$), here from $r = c_{1f} = 14 \mu\text{m}$ to $r = c_{2f} = 35 \mu\text{m}$.

A notable difference with post-mortem experimental observations has to be noted. With the parameters used here (see section 3.1), the delaminated area does not start from the symmetry axis. It is furthermore strictly confined below the indentation. In the experimental work, the delaminated area does start from the axis and its maximum extension $c > 139 \mu\text{m}$ (beyond the FIB section edge).

The mechanism displayed by the simulations with CZM involves a shear band which disconnects continuously oxide from substrate as it scans the interface outwards, following the increase of the indentation radius. The stress is concentrated, so that crack propagation does not extend beyond the shear stress band. Furthermore, at the beginning of indentation, say $p/t < 0.1$ or 0.2 , the plastic strain is strictly confined inside the oxide: all stresses are compressive, the shear band does not exist or does not extend to the interface. The crack first forms at 3.5 N load (indentation depth $11 \mu\text{m}$), when plasticity propagates to the substrate, promoting oxide bending. From then on, the crack tip propagates smoothly, exactly at the same place as the indentation radius and the shear stress band. This suggests that the central part of the interface in fact delaminates by an inward propagation during loading. Moreover, in experiments, crack propagation may be more brittle and sudden than given by the model, thus extending well beyond the shear stress band. It may be relevant to remind here that according to Marshall [19], the residual compressive stress enhance delamination of thin film during indentation ; here it is not considered.

From a more general point of view, remember that CZM is a crack propagation regularization, which bears an intrinsic danger to miss any sudden propagation, e.g. a crack jumping from defect to defect. The choice of the parameters is critical to avoid such dangers. In view of a better understanding, the influence of each CZM parameter is discussed in the next part.

4.3 Influence of CZM parameters

In this part, influence of critical shearing component and interfacial energy and CZM stiffness are discussed. All CZM parameters and corresponding simulations results (delaminated area) are described in Table 3.

4.3.1 G_c interfacial energy adhesion

Experimental work shows that interfacial energy adhesion G_c from eq.(1) is strongly dependant on steel grades: 45 and 330 J/m^2 for IF and HSLA respectively, the latter being known as “difficult to descale” contrary to the former. Applying these two values in numerical simulation, Abaqus® with CZM, we find no difference in delaminated area, which suggests either that eq.(1) does not describe the real

phenomenon or that G_c is not a representative variable for this model. Increasing G_c to 3300 J/m², the delaminated area is also the same. In such cases where, as soon as the critical stress is reached, CZM elements are immediately degraded (i.e. SDEG variable changes from 0 to 1 in one time step), G_c seems not to have any impact on the delamination process.

CZM parameters			Results	
Critical stress (MPa)	Interfacial Energy Adhesion (G_c)	Stiffness (GPa)	1 st delamination (% of max load)	Delaminated area (μm)
500	330	210	-	-
200	330	210	70	$c1_f=14$ $c2_f=35$
50	330	210	36	$c1_f=2$ $c2_f=54$
200	45	210	70	$c1_f=14$ $c2_f=35$
200	330	50/100/150	-	-
200	330	240	63	$c1_f=11$ $c2_f=38$

Table 3: Parametric study of CZM parameters and its results

4.3.2 Critical stress

Another key parameter is the critical stress t^0 (taken equal for the 3 components, see eq.(3)). When $t^0 = 500$ MPa, it is higher than any shear stress computed at the interface, so that no degradation is observed. By decreasing it to 50 MPa, the delaminated area is strongly modified. Indeed, the critical shearing component is reached sooner at the interface (36% of the loading i.e. 1.8 N, $p = 5,4 \mu\text{m}$, $a = 12 \mu\text{m}$, $p/t = 0.2$). Here, $c1_i=8 \mu\text{m}$ and $c2_i=15\mu\text{m}$. Then, delaminated area is increasing all along the loading. At the end of the indentation, it extends between $c1_f=2 \mu\text{m}$ and $c1_f=54 \mu\text{m}$. In this case, delaminated area is much closer to the experimental result ($\geq 70 \mu\text{m}$) and in both cases, it expands from the axis-symmetry to outside the contact area. It is interesting to note that here again, crack does not propagate upon unloading. This set of parameters suggests the initiation of the crack away from the axis and its extension in both directions (inward and outward), reaching the situation found post-mortem in the experimental case (Figure 1), providing deeper understanding of delamination of oxide during indentation test.

4.3.3 Elastic stiffness of CZM

In order to reduce the slope of elastic part of T-S law, stiffness properties can be modified. Initially, $E = E_{\text{steel}}$, Young's modulus of steel. When, $E < 150$ MPa, no delamination is observed because the stresses never reach the critical stresses t^0 . In the opposite way, when $E=240\text{GPa}$ ($=E_{\text{oxide}}$), delamination appears sooner and the final zone is larger: from $c1_f = 11\mu\text{m}$ to $c2_f = 38 \mu\text{m}$, to be compared with 14 and 35 μm with the first set of parameters.

To compare CZM parameters selected in our study, Noh et al. used cohesive elements to simulate spallation of oxide during a scratch test [29]. In their study, cohesive elements parameters were identified by an inverse method and critical stress components were set to $t_n^0=t_s^0=200$ MPa. This is why we took this value initially. For other parameters stiffness of cohesive elements equals to 200 GPa/ μm , fracture energy 18 J/m².

4.3.4 Discussion

This parametric study highlights influence of CZM parameters, pointing more precisely towards stress criterion. Surprisingly, the influence of G_c is not representative. It has no influence in spite of the wide range studied here: this first result will require confirmation. In addition, once critical stress is reached, usually, degradation of CZM is immediate, it means that energy stored in cohesive elements is very large; this is not the case however for extreme CZM values, namely very large G_c or low t_s^0 or stiffness. Choice of these parameters is crucial to simulate delamination of oxide at the interface. In our case, a correct parameter set for the IF steel seems to be: a critical stress of 50MPa, with G_c measured experimentally (330 J/m²) and elastic stiffness of 210 GPa.

Uncertain as it may be with its unknown parameters, the CZM model gives possible scenarios for the presence of the crack on the centreline. When indentation starts, plasticity is necessarily confined in the oxide as long as the “1/10th rule” is not violated ($p/t < 0.1$). Indeed, low load indentations do not display oxide delamination. Our expectation was that delamination would start at the centre when the inflating plastic zone reached it first and plasticity penetrated the steel substrate. Then the crack would have expanded outward more or less as the plastic zone did. What these simulations tell is different: the main stress component is the shear stress, and its maximum is not on the centre, but on the border of the plastic zone, roughly under the edge of the contact. Delamination thus starts away from the centreline, then, if the interface critical fracture stress is low, the crack will propagate in both directions and reach the centreline. Otherwise, the crack will remain annular as assumed by Rosenfeld et al. [9]. With our present set of experiments, it is difficult to validate one or the other scenario for this particular steel-oxide system, or to exhibit for which range of properties the central crack will be formed.

5. Conclusion

Room temperature indentation causes oxide to crack and delaminate. Thanks to FIB/SEM analysis, interfacial adhesion energy has been estimated using an analytical formula. Numerical simulations were carried out to refine the analysis. They explain localisation of cracks within oxide: circular cracks in surface, delamination at the interface and normal cracks in oxide initiated from the interface. At the interface between oxide and steel, CZM elements are implemented to allow delamination of oxide. The high shearing component due to indentation is suggested to be the main source of delamination, the axial stresses being compressive on the interface. In terms of CZM parameter, both elastic stiffness and critical stress to initiate delamination are the main parameters which influence the localisation of delaminated area and allow approaching experimental measurements.

In the model, due to the specificity of the early stage of indentation on such thick layers (26 μm), delamination occurs only after a certain depth so that the centre of the contact remains intact initially, then crack forms at a distance from the centreline and propagates inward and outward all along the loading to give the full circular cracks observed experimentally. This scenario deserves more parametric tests on the one hand, and in-situ monitoring of fracture propagation in experiments would be welcome on the other hand. The difficulty is that other crack families develop at the same time, which would e.g. blur interpretation of Acoustic Emission signal or of superficial micro-displacements.

Another point of interest would be the possible interactions between these different crack types: for instance, do cracks perpendicular to the interface start because of delamination, or do they appear first and facilitate delamination?

For the time being, the main perspective of this work is to reproduce the approach on high temperature indentation, bridging the gap with descaling.

Acknowledgement

The authors thank the French National Agency for Technological Research (ANRT), for the PhD grant of VCB, CIFRE #2019/1210.

References

- [1] Païdassi J. Sur la cinétique de l'oxydation du fer dans l'air dans l'intervalle 700–1250°C. *Acta Metallurgica* 1958; 6: 184–194.
- [2] Farrugia D, Richardson A, Lan YJ. Advancement in Understanding of Descalability during High Pressure Descaling. *Key Engineering Materials* 2014; 622–623: 29–36.
- [3] Raudensky M, Horak A, Horsky J, Pohanka M, Kotrbacek P. Hydraulic descaling improvement, findings of jet structure on water hammer effect. *Revue de Métallurgie – International Journal of Metallurgy* 2007; 104: 84–90.
- [4] Krzyzanowski M, Beynon JH. Modelling the Behaviour of Oxide Scale in Hot Rolling. *ISIJ International* 2006; 46: 1533–1547.
- [5] Filatov D, Pawelski O, Rasp W. Hot-Rolling Experiments on Deformation Behaviour of Oxide Scale. *steel research international* 2004; 75: 20–25.
- [6] Suárez L, Houbaert Y, Eynde XV, Colás R. High temperature deformation of oxide scale. *Corrosion Science* 2009; 51: 309–315.
- [7] PICQUÉ B. Experimental study and numerical simulation of iron oxide scales mechanical behavior in hot rolling. 2004.
- [8] Drory MD, Hutchinson JW. Measurement of the adhesion of a brittle film on a ductile substrate by indentation. *Proceedings of the Royal Society of London Series A: Mathematical, Physical and Engineering Sciences* 1996; 452: 2319–2341.
- [9] Rosenfeld LG, Ritter JE, Lardner TJ, Lin MR. Use of the microindentation technique for determining interfacial fracture energy. *Journal of Applied Physics* 1990; 67: 3291–3296.
- [10] Vlassak JJ, Drory MD, Nix WD. A simple technique for measuring the adhesion of brittle films to ductile substrates with application to diamond-coated titanium. *Journal of Materials Research* 1997; 12: 1900–1910.
- [11] Kriese MD, Gerberich WW, Moody NR. Quantitative adhesion measures of multilayer films: Part I. Indentation mechanics. *Journal of Materials Research* 1999; 14: 3007–3018.
- [12] Vasinonta A, Beuth JL. Measurement of interfacial toughness in thermal barrier coating systems by indentation. *Engineering Fracture Mechanics* 2001; 68: 843–860.
- [13] Kriese MD, Gerberich WW, Moody NR. Quantitative adhesion measures of multilayer films: Part II. Indentation of W/Cu, W/W, Cr/W. *Journal of Materials Research* 1999; 14: 3019–3026.
- [14] Hallett SR, Harper PW. 2 - Modelling delamination with cohesive interface elements. In: Camanho PP, Hallett SR, editors. *Numerical Modelling of Failure in Advanced Composite Materials*. Woodhead Publishing, 2015: 55–72.
- [15] Xiao Y, Shi W, Wan Q, Luo J. Evaluation of failure properties of a DLC/steel system using combined nanoindentation and finite element approach. *Diamond and Related Materials* 2019; 93: 159–167.
- [16] Park K, Paulino GH. Cohesive zone models: A critical review of traction-separation relationships across fracture surfaces. *Appl Mech Rev* 2011; 64: 061002.
- [17] Xu X-P, Needleman A. Numerical simulations of fast crack growth in brittle solids. *Journal of the Mechanics and Physics of Solids* 1994; 42: 1397–1434.
- [18] Abdul-Baqi A, Van der Giessen E. Numerical analysis of indentation-induced cracking of brittle coatings on ductile substrates. *International Journal of Solids and Structures* 2002; 39: 1427–1442.
- [19] Marshall DB, Evans AG. Measurement of adherence of residually stressed thin films by indentation. I. Mechanics of interface delamination. *Journal of Applied Physics* 1984; 56: 2632–2638.
- [20] Mougín J, Dupeux M, Antoni L, Galerie A. Adhesion of thermal oxide scales grown on ferritic stainless steels measured using the inverted blister test. *Materials Science & Engineering A* 2003; 1–2: 44–51.

- [21] Ahtoy E, Picard M, Leprince G *et al.* Time and temperature dependence of the adhesion of oxide scales formed on phosphorus-containing steels during short term oxidation. *Materials Chemistry and Physics* 2014; 148: 1157–1162.
- [22] Nilsonthi T, Chandra-ambhorn S, Wouters Y, Galerie A. Adhesion of Thermal Oxide Scales on Hot-Rolled Conventional and Recycled Steels. *Oxid Met* 2013; 79: 325–335.
- [23] Chandra-ambhorn S, Klubvihok N. Quantification of Adherence of Thermal Oxide Scale on Low Carbon Steel Using Tensile Test. *Oxid Met* 2016; 85: 103–125.
- [24] Chandra-ambhorn S, Ngamkham K, Jiratthanakul N. Effects of Process Parameters on Mechanical Adhesion of Thermal Oxide Scales on Hot-Rolled Low Carbon Steels. *Oxid Met* 2013; 80: 61–72.
- [25] Lee JH, Gao YF, Johanns KE, Pharr GM. Cohesive interface simulations of indentation cracking as a fracture toughness measurement method for brittle materials. *Acta Materialia* 2012; 60: 5448–5467.
- [26] Weppelmann E, Swain MV. Investigation of the stresses and stress intensity factors responsible for fracture of thin protective films during ultra-micro indentation tests with spherical indenters. *Thin Solid Films* 1996; 286: 111–121.
- [27] Krzyzanowski M, Beynon JH. Finite element model of steel oxide failure during tensile testing under hot rolling conditions. *Materials Science and Technology* 1999; 15: 1191–1198.
- [28] Tabor D. *The Hardness of Metals*. OUP Oxford, 1951.
- [29] Noh W, Lee J-M, Kim D-J, Song J-H, Lee M-G. Effects of the residual stress, interfacial roughness and scale thickness on the spallation of oxide scale grown on hot rolled steel sheet. *Materials Science and Engineering: A* 2019; 739: 301–316.
- [30] Schütze M. Mechanical properties of oxide scales. *Oxid Met* 1995; 44: 29–61.
- [31] Huntz AM, Schütze M. Stresses generated during oxidation sequences and high temperature fracture. *Materials at High Temperatures* 1994; 12: 151–161.
- [32] Marshall DB, Lawn BR, Evans AG. Elastic/Plastic Indentation Damage in Ceramics: The Lateral Crack System - MARSHALL - 1982 - *Journal of the American Ceramic Society* - Wiley Online Library. *Journal of the American Ceramic Society* 1982; 65: 561–566.
- [33] Claverie-Burgué V, Montmitonnet P, Inal K, Burr A, Picard M and Settefrati A, Micro-Indentation of oxidized low carbon steel to evaluate properties of oxides. *Proc. 19th Metal Forming Conference* (11-14 Sept. 2022, Taiyuan, P.R. China), to be published in IOP Conf. Series: Mat. Sci. & Engg.